Wake effect and stopping power for a charged ion moving in magnetized two-component plasmas: Two-dimensional particle-in-cell simulation

Zhang-Hu Hu, Yuan-Hong Song, and You-Nian Wang*
School of Physics and Optoelectronic Technology, Dalian University of Technology, Dalian 116024, People's Republic of China
(Received 2 April 2010; revised manuscript received 14 June 2010; published 16 August 2010)

A two-dimensional particle-in-cell (PIC) model is proposed to study the wake field and stopping power induced by a nonrelativistic charged particle moving perpendicular to the external magnetic field in two-component plasmas. The effects of the magnetic field on the wake potential and the stopping due to the polarization of both the plasma ions and electrons are discussed. The velocity fields of plasma ions and electrons are investigated, respectively, in the weak and strong magnetic field cases. Our simulation results show that in the case of weak magnetic field and high ion velocity, the wakes exhibit typical V-shaped cone structures and the opening cone angles decrease with the increasing ion velocity. As the magnetic field becomes strong, the wakes lose their typical V-shaped structures and become highly asymmetrical. Similar results can be obtained in the case of low ion velocity and strong magnetic field. In addition, stopping power is calculated and compared with previous one-dimensional and full three-dimensional PIC results.

DOI: 10.1103/PhysRevE.82.026404 PACS number(s): 52.40.Mj, 34.50.Bw, 52.25.Xz

I. INTRODUCTION

The interaction of particles and plasmas, including the dynamics of charged particles moving through plasmas, the subsequent slowing-down process due to the interaction with the background electrons and ions, and the excitation of plasma waves have been studied by a number of authors since the early 1950s [1–3]. The so-called stopping power and wake potential induced by the charged particle have been a topic of great interest due to their many applications, such as the inertial confinement fusion driven by ion beams [4–6] and the cooling of heavy-ion beams by electrons [7,8]. In addition, the structure of the wake field is found to be important for the determination of the correlations in ion clusters [9].

The interaction process is usually characterized with the ion-plasma coupling strength $Z=Z_p/N_D$, where Z_p is the charge of the ion and N_D is the number of electrons in a Debye sphere. For weak ion-plasma coupling $Z \ll 1$, the well-known linearized theories, such as the dielectric and binary collision theories, are commonly adopted to investigate the wake potential and energy loss. The reaction of a uniform plasma to the electrostatic field induced by a moving test electron was first studied by Rostoker and Rosenbluth [2]. It is shown that the emission of electron plasma waves with a given k is concentrated on the cone, forming an angle θ with respect to the test electron velocity $\mathbf{v}_0$, where $\cos\theta = \omega_{pe}/v_0 k$. For the magnetized plasmas, the external magnetic field plays an important role on the wake potential and stopping power [10–12]. For ions traveling parallel to the magnetic field, the magnitude of the wake potential is found to increase significantly with the increasing magnetic field. Meanwhile, the dynamic polarization effects of plasma ions become obvious and contribute mainly to the stopping power for the case of strong magnetic field and low projectile velocities [12].

For strong ion-plasma coupling $Z \gtrsim 1$, the standard linearized theories fail. In these studies, particle-in-cell (PIC), molecular-dynamics [13–16], and Vlasov [17] simulations are usually employed to study the influences of nonlinear effects on the interaction process. It is demonstrated that the nonlinear effects on the wake field induced behind the ion are weaker than those predicted by the dielectric theory due to strong electron deflection by the self-consistent potential humps [17]. Comparing the molecular-dynamics simulations with those in the dielectric theory, the nonlinear effects are found to enhance the stopping power at low ion velocities [16]. This enhancement has been shown to be at most 10% of the linear results. Furthermore, the nonlinear stopping power for ions moving in the magnetized two-component plasmas is investigated through the PIC simulations [18]. In this work, the enhancement of the stopping power in the low-velocity regions due to the nonlinear effects is found when comparing the simulation results with the dielectric theory.

However, as far as we know, there are few investigations on the influences of the external magnetic field on the wake field in the strong ion-plasma coupling case. Actually, the structure of the wake field is important in many applications, such as plasma wake-field accelerator [19] and the stopping of ion clusters in plasmas [9]. The aim of this paper, which is an extension of our previous one-dimensional (1D) work [18], is to investigate the influences of the magnetic field on the wake field by using the two-dimensional (2D) PIC simulations, taking into account the dynamic polarization effects of both plasma ions and electrons. Investigations on the nonlinear stopping power of the charged particles are also carried out. The paper is organized as follows. In Sec. II, two-dimensional PIC simulation methods are briefly described. The influences of the magnetic field on the wake field are discussed in Sec. III. In Sec. IV, the stopping power of the charged ion obtained from the two-dimensional PIC simulations is analyzed and compared to 1D and full three-dimensional (3D) PIC simulations. Finally, we give a short summary in Sec. V.

*ynwang@dlut.edu.cn

II. PIC SIMULATION METHODS

Consider a Cartesian coordinate system with $\mathbf{r}=\{x,y,z\}$, which is immersed in a large volume of magnetized plasmas with electron density n_0. The magnetic field $\mathbf{B}_0$ applied in the plasma is homogeneous and directed along the z axis. Now consider a test particle with charge $Z_p e$ and velocity $\mathbf{u}$ moving in the magnetized plasma at an angle θ_0 with respect to the magnetic field $\mathbf{B}_0$. The equations of motion for plasma electrons and ions are

$$\frac{d\mathbf{r}_j^\alpha}{dt} = \mathbf{v}_j^\alpha, \tag{1}$$

$$\frac{d\mathbf{v}_j^\alpha}{dt} = \frac{Z_\alpha e}{m_\alpha}(\mathbf{E}_{ind} + \mathbf{E}_{ext} + \mathbf{v}_j^\alpha \times \mathbf{B}_0), \quad j = 1,2,\ldots,N_\alpha, \tag{2}$$

and the equations of motion for the test particle are

$$\frac{d\mathbf{R}}{dt} = \mathbf{u}, \tag{3}$$

$$\frac{d\mathbf{u}}{dt} = \frac{Z_p e}{m_p}(\mathbf{E}_{ind} + \mathbf{u} \times \mathbf{B}_0). \tag{4}$$

Here, $\mathbf{r}_j^\alpha$, $\mathbf{v}_j^\alpha$, Z_α, and m_α are the position, velocity, charge, and mass of plasma electrons ($\alpha=e$) and ions ($\alpha=i$), respectively. $\mathbf{R}$ and m_p are the position and mass of the test particle. The induced electric field $\mathbf{E}_{ind}=-\nabla\phi_{ind}$ is determined by the Poisson's equation

$$\nabla \cdot \mathbf{E}_{ind} = \frac{\rho_{ind}}{\varepsilon_0}, \tag{5}$$

and the external field $\mathbf{E}_{ext}$ generated by the test particle is expressed as

$$\mathbf{E}_{ext} = -\nabla\phi_{ext} = -\nabla\left(\frac{Z_p e}{4\pi\varepsilon_0|\mathbf{r}_j - \mathbf{R}|}\right). \tag{6}$$

A 2D3V electrostatic PIC code is used for the simulations. All the charged particles, including the test particle, are considered to move in the x-y plane. Therefore, only the case of a test particle moving perpendicular to the external magnetic field is considered in the present work. The present 2D model, in which all charged particles are represented by rods extending along z direction, is shown in Fig. 1. The simulation box is composed of $N_x=128$ grids in the x direction and $N_y=64$ grids in the y direction. We have adopted averaged 100 superparticles per cell, which has been varied to check the stability of the results. To simulate an infinite plasma, we take periodic boundary conditions in both x and y directions. The "area weighting" technique is used to deposit the charge on the four nearest grid points in order to obtain the spatial distribution of the particles on the mesh. The numerical integration of the motion equations for all charged particles is performed by a standard leap-frog algorithm, and the Lorentz forces in Eqs. (2) and (4) are treated with the Boris rotation

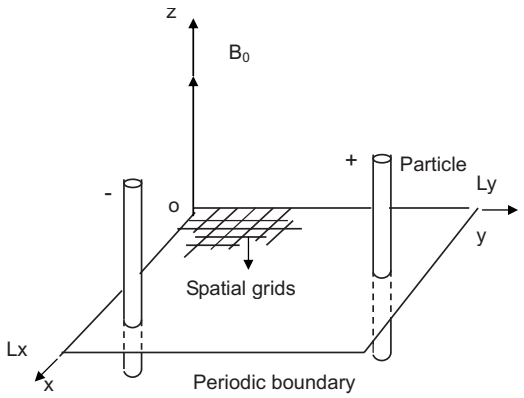

FIG. 1. 2D plasma model.

[20]. The Poisson's equation is solved in Fourier space by using the fast Fourier transformation to switch forth and back. Digital filtering of grid quantities is generally used in simulations in order to improve the overall accuracy and reduce the numerical noise [20]. Different methods of initial particle loading are used to check the influences on the numerical results. As shown later, this influence is negligible. Also, to reduce the numerical noise, an average over the stopping power is taken from various runs with the same coupling parameters β_e, β_i, test ion charge Z_p, and ion velocity u, but different initial positions of the test ion. The accuracy and the stability of the runs are monitored using the total energy and moment.

Let $\mathbf{u}_{e1}(\mathbf{r},t)$ and $\mathbf{u}_{i1}(\mathbf{r},t)$ be, respectively, the velocity fields of plasma electrons and ions at the position $\mathbf{r}=\{k\Delta x, m\Delta y\}$ and at time t, where $k=0,1,\ldots,N_x$ and $m=0,1,\ldots,N_y$. Here, Δx and Δy are the grid sizes in the x and y directions. Thus, the velocity field $\mathbf{u}_{\alpha 1}^{k,m}$ at the grid points (k,m) and at time t is obtained from the particle velocity located at positions $\mathbf{r}_j^\alpha=(x_j^\alpha, y_j^\alpha)$ from

$$\mathbf{u}_{\alpha 1}^{k,m} = \sum_{j=1}^{N_\alpha} \mathbf{v}_j^\alpha S(X_k - x_j^\alpha, Y_m - y_j^\alpha), \quad \alpha = e,i. \tag{7}$$

Here, S is the weighting function, with $X_k=k\Delta x$ and $Y_m=m\Delta y$. In the calculations, we use the same weighting functions S as in the charge density and force weighting.

For a two-component plasma, we have two parameters, $\beta_e=Z_p/n_0\lambda_{De}^3$ and $\beta_i=Z_p/n_0\lambda_{Di}^3$, characterizing, respectively, the coupling strength between the test particle and the plasma electrons and ions. In our numerical calculations, the coupling parameters $\beta_e=1.0$, $\beta_i=2.8$ and the ion charge $Z_p=5$ are kept fixed, and the speed of the projectile u and the external magnetic field B_0 are treated as variable parameters. Here, a hydrogen plasma with mass ratio $m_i/m_e=1836$ and ion charge $q=e$ is considered. In addition, the temperature ratio of ion to electron is assumed to be 0.5 ($T_i/T_e=0.5$). In the simulation, a boron ion of charge $Z_p=5$ and mass $m_p=10m_i$ is taken to be the test particle. The presented values of β_e and β_i refer to electron density $n_0\approx 10^{22}$ cm^{-3}, electron temperature $T_e\approx 20$ eV, and ion temperature $T_i\approx 10$ eV in a heavy-ion fusion experiment or $n_0\approx 10^8$ cm^{-3}, T_e

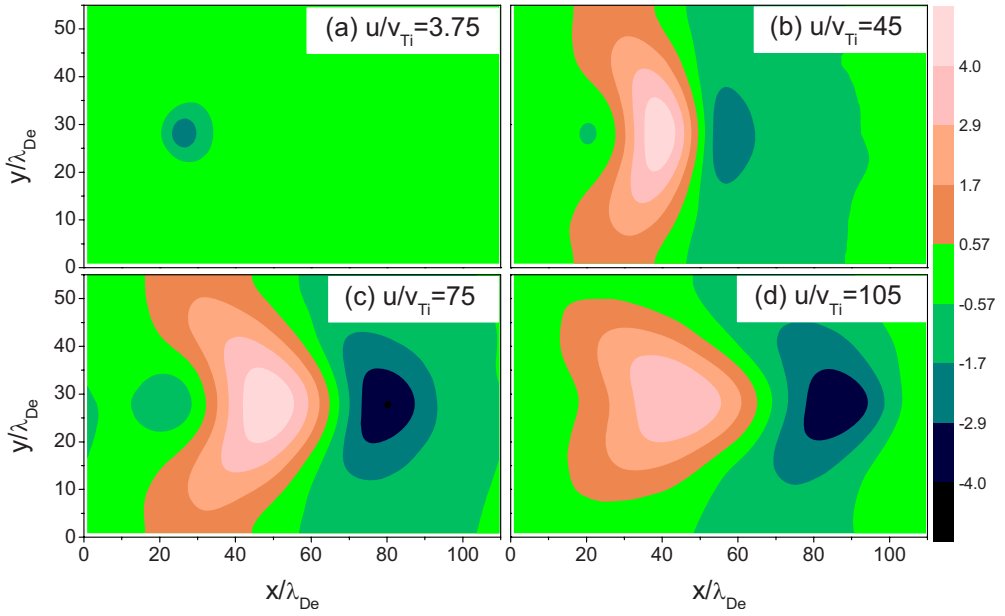

FIG. 2. (Color online) The induced potential ϕ_{ind} (normalized by $k_B T_e/e$) in the wake-field region created by the test ion for different ion velocities: u/v_{Ti}= (a) 3.75, (b) 45, (c) 75, and (d) 105, in the case of weak magnetic field η=0.01.

$\approx$0.5 meV, and $T_i \approx 0.25$ meV in an electron cooler. The angle θ_0 between the projectile velocity $\mathbf{u}$ and the external magnetic field $\mathbf{B}_0$ is taken to be $\pi/2$.

In the simulations, the intensity of the magnetic field B_0 is expressed in terms of $\eta=\omega_{ce}/\omega_{pe}$, where $\omega_{ce}=eB_0/m_e$ is the cyclotron frequency and $\omega_{pe}=(n_0e^2/\varepsilon_0 m_e)^{1/2}$ is the plasma frequency. We have $\eta \ll 1$ for weak magnetic fields and $\eta \geq 1$ for strong magnetic fields. For simplicity we assume that the test ion moves in the direction of positive x axis. Moreover, the following dimensionless variables are adopted: $r \rightarrow r/\lambda_{De}$, $u \rightarrow u/v_{Te}$, $t \rightarrow t\omega_{Pe}$, $\phi \rightarrow e\phi/k_B T_e$, and $n \rightarrow n/n_0$, where $\lambda_{De}=\sqrt{\varepsilon_0 k_B T_e/n_0 e^2}$ is the Debye length of the plasma electrons, $v_{Te}=\sqrt{k_B T_e/m_e}$ is the thermal velocity of plasma electrons, k_B is the Boltzmann constant, and T_e and T_i are the electron and ion temperatures, respectively.

III. WAKE EFFECTS

We regard the plasma as an assembly of charged particles, which in two dimensions are represented by rods extending along the z axis, immersed in a uniform magnetic field $\mathbf{B}_0$ (shown in Fig. 1). In the present 2D model, motion in the z direction is allowed and five coordinates are carried for each particle, namely (x, y, v_x, v_y, v_z), which goes partway to a 3D model. In the present configuration, the Lorentz force in the z direction is zero. Thus, the symmetry of the wake field along the z direction can be expected. The wake field obtained from the present 2D model can be interpreted as the wake field at the z=0 plane of the real 3D model. Also, there are circumstances in which real plasma may behave very like a 2D system. In magnetized plasmas, as all charges in plasmas on a given flux tube tend to remain together; the flux tubes and the particles on them retain their identities [21]. When a test ion is injected into the plasma and travels perpendicular to the external magnetic field, the plasma acquires an imbalance of charge between various flux tubes. Then these flux tubes would behave exactly as the charge rods of the present 2D model. Thus, we believe that the present 2D model can give some valuable results for the related experiments and applications.

Now we analyze the influences of the magnetic field on the wake field. We first show in Fig. 2 the induced potential ϕ_{ind} (normalized by $k_B T_e/e$) in the wake-field region for different ion velocities: u/v_{Ti}=3.75 [Fig. 2(a)], 45 [Fig. 2(b)], 75 [Fig. 2(c)], and 105 [Fig. 2(d)], in the case of weak magnetic field η=0.01. One can clearly see from this figure that, for low ion velocity u/v_{Ti}=3.75, it presents an almost symmetric profile around the test particle, compared with those in high ion velocity cases shown in Figs. 2(b)–2(d), in which the V-shaped cone structures lag apparently behind the ion, along with multiple oscillatory lateral wakes. Besides, it can be seen that these structures are composed of multiple cones and the cone wings are perpendicular to the direction of the ion motion. Moreover, the cone opening angle is seen in this figure to decrease with the increasing ion velocity. Figures 3 and 4 show the perturbed density n_{e1} (normalized by n_0) and velocity field $\mathbf{u}_{e1}$ of the electrons in the wake-field region, respectively, with the same parameters as in Fig. 2. The main features observed in Fig. 2 are reproduced in both figures.

We further show in Fig. 5 the influences of the magnetic field on the induced potential ϕ_{ind} (normalized to $k_B T_e/e$) with the ion velocity u/v_{Ti}=75. We observe from this figure that, as the magnetic field increases, the wake profiles become highly asymmetrical and lose their typical V-shaped cone structures, in contrast to the weak magnetic field case as shown in Fig. 2(c). As we all know, under the influences of the strong magnetic field, the test ion may experience much greater Lorentz force and leave its original motion trajectory. Thus, as the test ion travels through the plasma, one can expect the asymmetry in the wake potential induced behind the ion. Besides, with the increasing magnetic field, the mag-

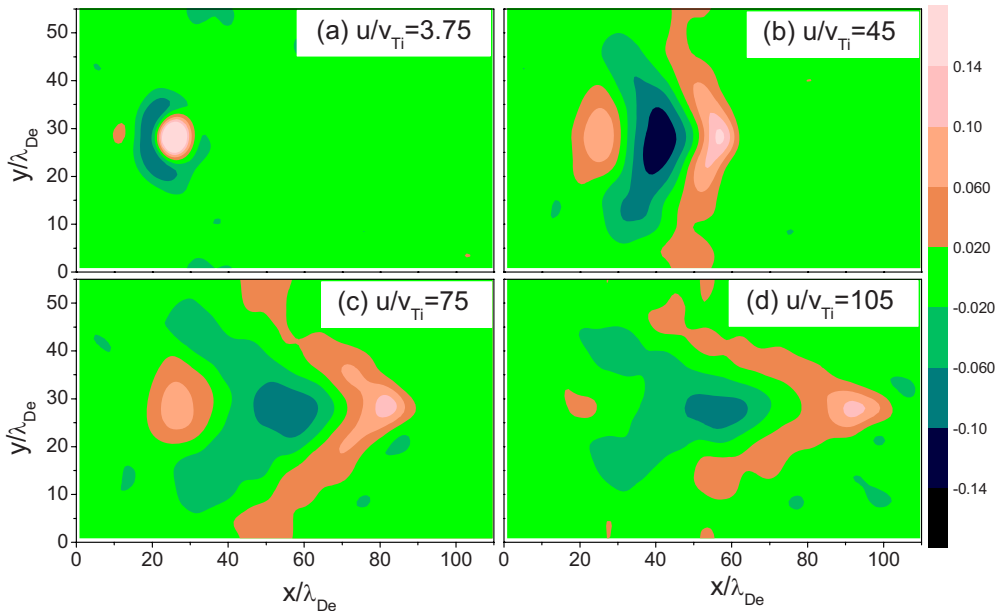

FIG. 3. (Color online) The perturbed density of plasma electrons n_{e1} (normalized by n_0) in the wake-field region for the same parameters as in Fig. 1.

nitude of the wake potential increases and the perturbed regions become smaller, as shown in Figs. 5(c) and 5(d). In our opinion, the motion of the plasma electrons is increasingly restricted under the influences of stronger magnetic field. In this case, the electrons cannot respond thoroughly to the disturbance from the intrusive ion, resulting in the reduction in the wake region. Also, we can observe these features from the maps of the perturbed density n_{e1} and velocity field $\mathbf{u}_{e1}$ of plasma electrons, as shown in Figs. 6 and 7. The asymmetry of the perturbed density and velocity field can be easily seen, especially from Figs. 6(d) and 7(d).

Furthermore, Fig. 8 shows the influences of strong magnetic fields on the velocity field $\mathbf{u}_{i1}$ of plasma ions in the case of low projectile velocity $u/v_{Ti}=3$, where the projectile can interact strongly with plasma ions. The similar cone structures of the velocity field in the wake-field regions are reproduced in the case of relative small magnetic field in Fig. 8(a), showing the obvious dynamic polarization of plasma ions. As the magnetic field becomes stronger, we can see the asymmetric interaction region in the other figures, indicating the enhancement of the dynamic polarization with the increasing magnetic field. These show good agreement with

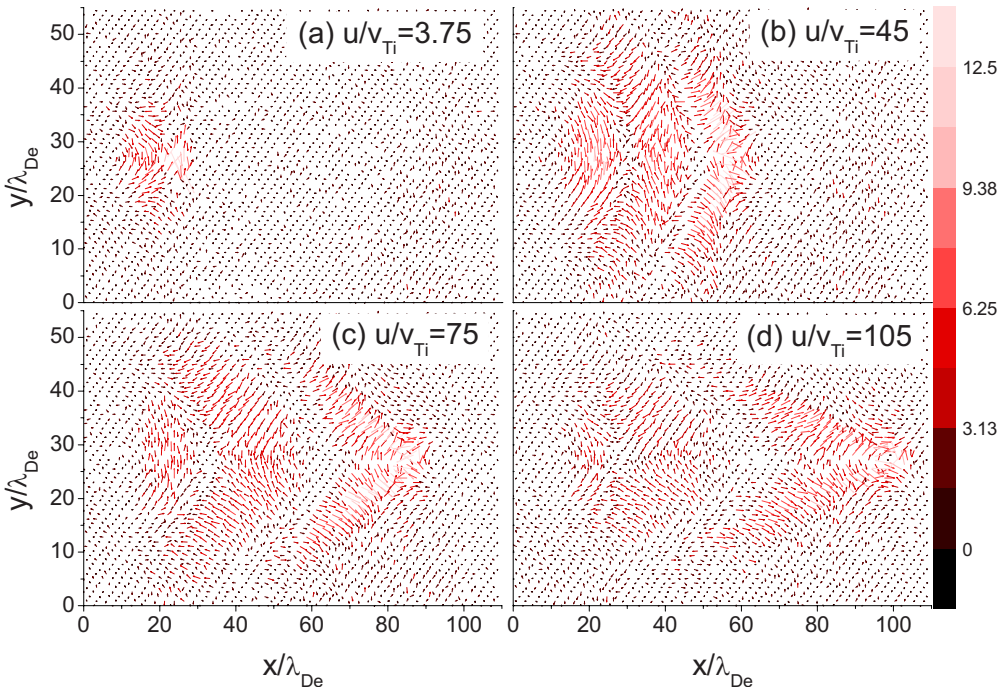

FIG. 4. (Color online) Velocity field of plasma electrons $\mathbf{u}_{e1}$ in the wake-field region for the same parameters as in Fig. 1.

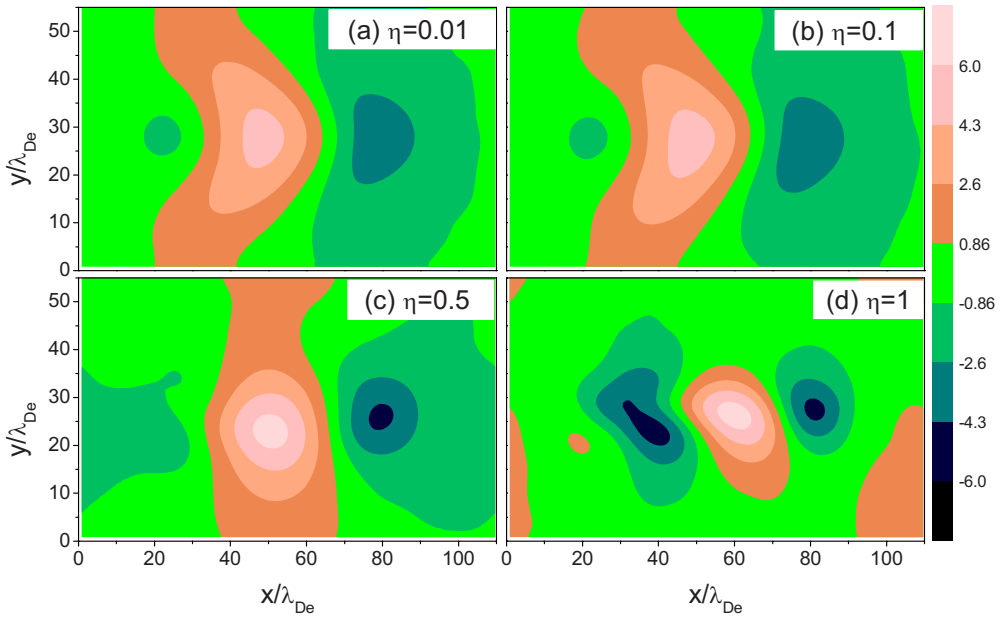

FIG. 5. (Color online) Influences of the magnetic field on the induced potential ϕ_{ind} (normalized by $k_B T_e/e$), with the ion velocity $u/v_{Ti}=75$.

the conclusion from our previous work [12,18], in which the dynamic polarization effects of plasma ions are shown to be important for low projectile velocities and strong magnetic fields, while in high projectile velocity regions, as shown in Fig. 7, the dynamic polarization of plasma electrons becomes obvious.

IV. STOPPING POWER

The energy loss of the projectile per unit path length, or its stopping power, is an important quantity for describing the interactions of ions with plasmas. We also calculate the stopping power of ions in our two-dimensional PIC simulations and compare these with the results of our previous one-dimensional work. In the simulations, the energy loss ΔE and the traveled path Δs of the test particle are calculated at each time step, resulting in an instantaneous stopping power $(\Delta E/\Delta s)(t)$. The stopping power is finally obtained as the time average $\langle \Delta E/\Delta s \rangle$ over the instantaneous $\Delta E/\Delta s$. We first show in Fig. 9 the influences of the weak and strong magnetic fields on the nonlinear stopping power as a function of the projectile velocity u/v_{Ti}. Here, the stopping

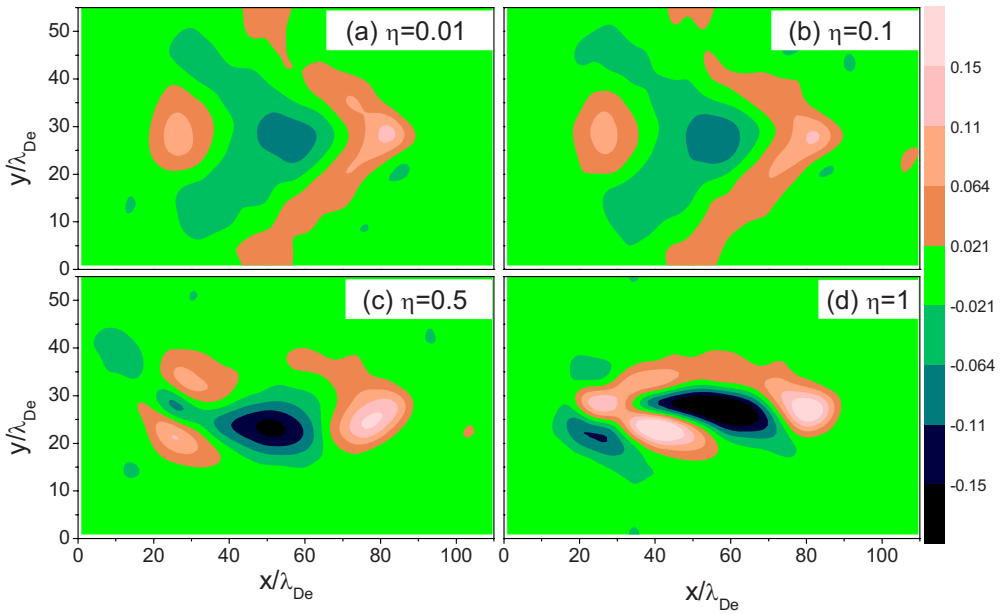

FIG. 6. (Color online) Influences of the magnetic field on the perturbed density of plasma electrons n_{e1} (normalized by n_0) for the same parameters as in Fig. 5.

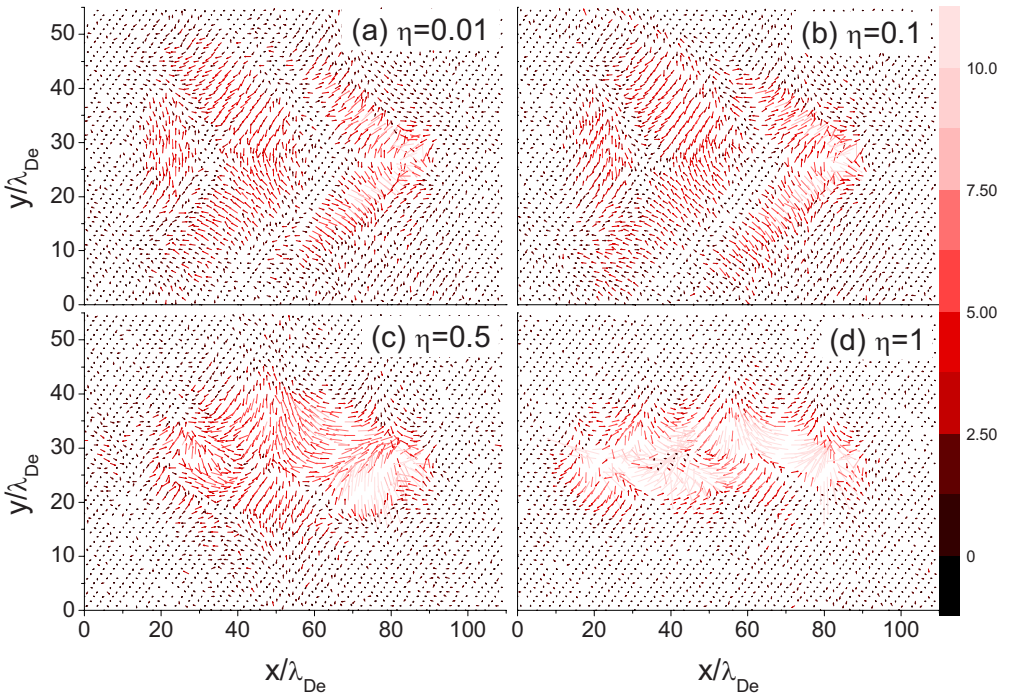

FIG. 7. (Color online) Influences of the magnetic field on the velocity field of plasma electrons $\mathbf{u}_{e1}$ for the same parameters as in Fig. 5.

power is normalized in units of $S_0=(Z_p e)^2/4\pi^2\varepsilon_0\lambda_{De}^2$. Similar to our previous 1D model [18], two characteristic peaks corresponding to the ion stopping in low-velocity region and the electron stopping in high-velocity region are displayed. Also, one can clearly see the significant enhancement of the stopping power with increasing magnetic field at high ion velocity region due to the strong dynamic polarization of plasma electrons in Fig. 9(a) and also at the low ion velocity region due to the plasma ion excitation in Fig. 9(b).

The comparison of the stopping power between the one- and two-dimensional models is made in Fig. 10 with the weak, $\eta=0.1$, and strong, $\eta=5$, magnetic fields, respectively. In the case of strong magnetic field in Fig. 10(b) one can find that, at the high ion velocity region the two simulations for

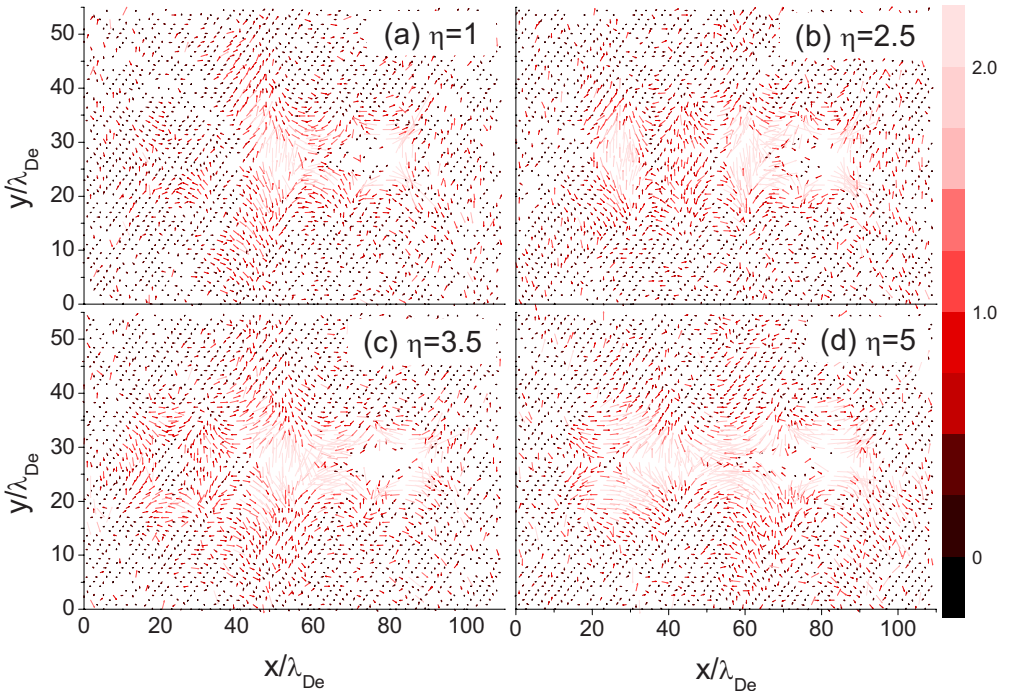

FIG. 8. (Color online) Influences of strong magnetic field on the velocity field of plasma ions $\mathbf{u}_{i1}$ in the case of low projectile velocity $u/v_{Ti}=3$.

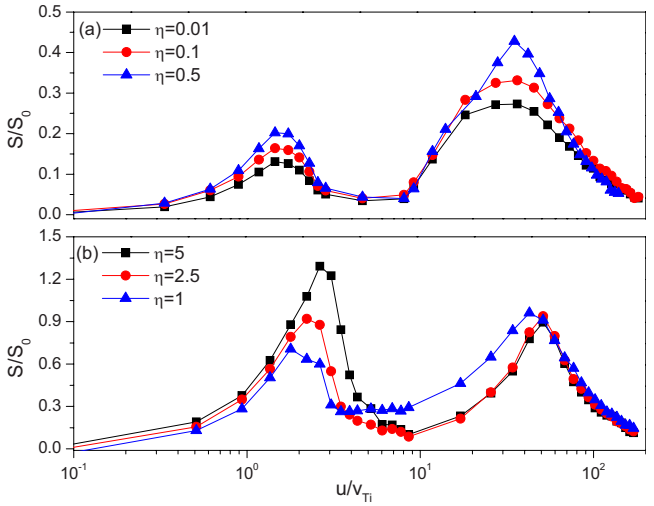

FIG. 9. (Color online) Influences of the weak and strong magnetic fields on the nonlinear stopping power [in units of $S_0=(Z_pe)^2/4\pi^2\varepsilon_0\lambda_{De}^2$], as a function of the projectile velocity u/v_{Ti}.

the electron stopping show agreement with each other, while at the low ion velocity region, the peak of ion stopping in two-dimensional model moves to higher-velocity region, relative to former 1D results. For weak magnetic field, a reversed behavior can be observed. By adopting the two-dimensional PIC simulation model in this work, we can obtain the highly asymmetrical results for both the induced potential and the velocity field in x and y directions, as shown in the last section. Thus, one can expect that the differences of the simulation results between the two models are due to the action of the magnetic field on the plasma ions and electrons at their sensitive velocity region, in a 2D fashion.

Furthermore, simulation results are compared with the full 3D PIC results, presented in Ref. [16], in order to show the

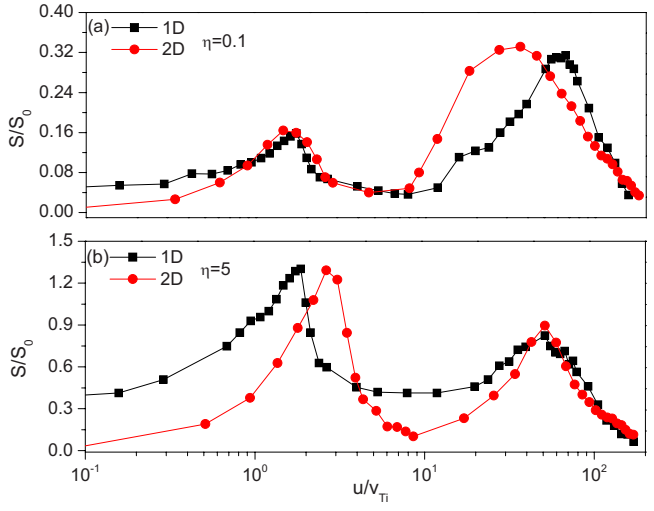

FIG. 10. (Color online) Comparisons of the stopping power [in units of $S_0=(Z_pe)^2/4\pi^2\varepsilon_0\lambda_{De}^2$] between 1D and 2D PIC simulations in the cases of weak, $\eta=0.1$, and strong, $\eta=5$, magnetic fields. Here, the lines with filled squares are the results of 1D model; the lines with filled circles are those of 2D model.

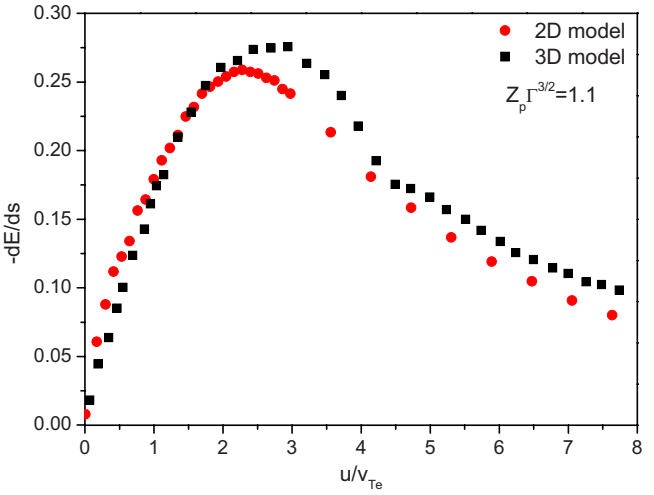

FIG. 11. (Color online) Comparisons of the normalized stopping power $dE/ds/(Z_p\Gamma^{3/2})^2$ in units of $\sqrt{3}k_BT_e/\Gamma^{3/2}\lambda_{De}$ as a function of ion velocity u/v_{Te} between 2D and full 3D PIC models. Here, the coupling parameter $Z_p\Gamma^{3/2}=Z_pe^2\omega_{pe}/(4\pi\sqrt{3}\varepsilon_0k_BT_ev_{Te})=1.1$ and the 3D results are corrected for the finite simulation box, as indicated in Ref. [16]. The filled squares are the results of full 3D model; the filled circles are those of 2D model.

differences between the present 2D and the real 3D models. We first calculate the normalized stopping power $dE/ds/(Z_p\Gamma^{3/2})^2$ in units of $\sqrt{3}k_BT_e/\Gamma^{3/2}\lambda_{De}$ as a function of ion velocity u/v_{Te} in Fig. 11 for vanishing magnetic field and one-component plasma, as indicated in Fig. 2 of Ref. [16]. Here, the coupling parameter $Z_p\Gamma^{3/2}=Z_pe^2\omega_{pe}/(4\pi\sqrt{3}\varepsilon_0k_BT_ev_{Te})=1.1$ and the 3D results are corrected for the finite simulation box. One can see from this figure that the overall difference is small, although some reduction in the stopping power in high ion velocity regions can be found in the present 2D model. As one can see in high ion velocity regions plasma waves are greatly excited by the test ion and the wake effects induced behind the ion are expected to be obvious. Thus, some differences can be expected due to certain missing information about the wake fields and plasma waves along the z direction in the present 2D model, in which the particle trajectory in the z direction cannot be tracked.

V. SUMMARY

Two-dimensional particle-in-cell simulations are performed to investigate the wake field and the stopping power induced by test particles in magnetized two-component plasmas. Special attention is paid on the influences of the magnetic field on the wake potential behind test particles. For relatively high ion velocity and weak magnetic field, our simulation results show that the wake field excited by moving ions exhibits typical V-shaped cone structures and the opening cone angles decrease as the ion velocity increases. In such a case the dynamic polarization of plasma electrons is important and the plasma ions are just polarized along the trajectory of the projectile. As the magnetic field increases, the wake tails lose their V-shaped structures gradually and

become highly asymmetrical. Besides, the magnitude of the wake field increases and the perturbed regions caused by the moving ions get smaller due to strong restriction on electron motion. Similar simulation results are obtained for relatively low ion velocity and strong magnetic field; in such a case, the plasma ion polarization plays the major role relative to the plasma electron one.

In the stopping power calculation, the main conclusions already reached in the previous 1D work is essentially confirmed in the present 2D one. However, the location of the stopping peaks is expected to move in this latter case, either through plasma ion polarization in low ion velocity region with strong magnetic field or through plasma electron excitation in the high ion velocity region under the action of a weak magnetic field. Comparisons with the full 3D PIC model are also made (for vanishing magnetic field and one-component plasma) and the overall difference is found to be small. Our future attention will concentrate on a real 3D plasma model in the presence of external magnetic fields.

ACKNOWLEDGMENTS

This work was supported by the National Basic Research Program of China (Grants No. 2010CB832901 and No. 2008CB717801) and the Fundamental Research Funds for the Central Universities (Grant No. DUT10ZD111).

[1] D. Pines and D. Bohm, Phys. Rev. **85**, 338 (1952).
[2] N. Rostoker and M. N. Rosenbluth, Phys. Fluids **3**, 1 (1960).
[3] S. T. Butler and M. J. Buckingham, Phys. Rev. **126**, 1 (1962).
[4] D. Keefe, Ann. Rev. Nucl. Part. Sci. **32**, 391 (1982).
[5] C. Deutsch, Ann. Phys. (Paris) **11**, 1 (1986).
[6] T. Peter and J. Meyer-ter-Vehn, Phys. Rev. A **43**, 1998 (1991).
[7] H. Poth, Phys. Rep. **196**, 135 (1990).
[8] I. N. Meshkov, Phys. Part. Nucl. **25**, 631 (1994).
[9] J. D'Avanzo, M. Lontano, and P. F. Bortignon, Phys. Rev. A **45**, 6126 (1992).
[10] A. A. Ware and J. C. Wiley, Phys. Fluids B **5**, 2764 (1993).
[11] C. Deutsch and R. Popoff, Phys. Rev. E **78**, 056405 (2008).
[12] Z.-H. Hu, Y.-H. Song, and Y.-N. Wang, Phys. Rev. E **79**, 016405 (2009).
[13] G. Zwicknagel, C. Toepffer, and P.-G. Reinhard, Hyperfine Interact. **99**, 285 (1996).
[14] J. D'Avanzo, I. Hofmann, and M. Lontano, Nucl. Instrum. Methods Phys. Res. A **415**, 632 (1998).
[15] G. Zwicknagel, C. Toepffer, and P.-G. Reinhard, Phys. Rep. **309**, 117 (1999).
[16] G. Zwicknagel, Nucl. Instrum. Methods Phys. Res. B **197**, 22 (2002).
[17] O. Boine-Frankenheim, Phys. Plasmas **3**, 1585 (1996).
[18] Z.-H. Hu, Y.-H. Song, G.-Q. Wang, and Y.-N. Wang, Phys. Plasmas **16**, 112304 (2009).
[19] J. B. Rosenzweig, Phys. Rev. Lett. **58**, 555 (1987).
[20] R. W. Hockney and J. W. Eastwood, *Computer Simulation Using Particles* (McGraw-Hill, New York, 1981), Secs. 3.5 and 4.4.
[21] J. B. Taylor and B. Mcnamara, Phys. Fluids **14**, 1492 (1971).